Towards spin experiments with magnetic resonance force microscopy: characterizing frequency shifts and frequency uncertainties

Winter, Myrthe de

Towards spin experiments with magnetic resonance force microscopy: characterizing frequency shifts and frequency uncertainties

THESIS

submitted in partial fulfillment of the
requirements for the degree of

BACHELOR OF SCIENCE
in
PHYSICS

Author :	M.A. de Winter
Student ID :	s3318605
Supervisor :	Prof.dr.ir. T.H. Oosterkamp
	Ir. L.R. van Everdingen
Second corrector :	Dr.ir. B.J. Hensen

Leiden, The Netherlands, August 1, 2025

Towards spin experiments with magnetic resonance force microscopy: characterizing frequency shifts and frequency uncertainties

M.A. de Winter

Huygens-Kamerlingh Onnes Laboratory, Leiden University
P.O. Box 9500, 2300 RA Leiden, The Netherlands

August 1, 2025

Abstract

A way to test models of spontaneous wavefunction collapse is through the creation of a macroscopic quantum superposition. A potential method for achieving such a superposition involves coupling a cantilever to a single spin in superposition using Magnetic Resonance Force Microscopy (MRFM). As an initial step towards this goal, it is necessary to be able to detect spins through cantilever frequency shifts. In this thesis, we present a method for positioning the cantilever. We find an inverse relation between the cantilever's driving voltage and its frequency uncertainty. We also observe that frequency uncertainty depends on the cantilever's position, but shows no clear dependence on temperature. Finally, we develop a model to describe frequency shifts due to the Meissner effect, but show that it does not align with experimental observations.

Contents

Version of August 1, 2025– Created August 1, 2025 - 13:51

Chapter 1

Introduction

Quantum mechanics has been proven to be very successful for describing physical phenomena on small scales [1], while Einstein's theory of general relativity [2] is crucial for describing the universe on the largest distance scales [3]. General relativity is a local and causal theory, whereas the quantum mechanical collapse of a wavefunction is nonlocal, it influences the entire wavefunction at once [4]. Currently, there is no unification between these theories [5].

A way to find a relation between general relativity and quantum mechanics is through experimentally testing models of spontaneous wave function collapse. These models suggest a more general theory of quantum mechanics, where the current theory is just an approximation of [1]. One way to test these models is through macroscopic superposition [6].

In the Oosterkamp lab, we work towards creating a macroscopic superposition using Magnetic Resonance Force Microscopy (MRFM) at an extremely low temperature. The goal is to couple a mechanical resonator, a cantilever with a magnetic tip, to a single spin in superposition. Because a spin, depending on its orientation, influences the resonance frequency of the cantilever, a spin in superposition would influence the mechanical resonator in two different ways at the same time. Thus bringing the macroscopic mechanical resonator in superposition [7].

Coupling a mechanical resonator to a single spin has been done before at a temperature of 1.6 K with detection of the oscillation of the mechanical resonator through a laser interferometer [8]. However, for reaching a quantum superposition of a mechanical resonator, a temperature of 1 mK is proposed [7]. As a laser would cause too much heat at this temperature [9], a Superconducting Quantum Interference Device (SQUID) with a superconducting pickup loop is used to detect the oscillation of the me-

chanical resonator [10].

Before coupling the cantilever to a single spin, we need to be able to measure spins in general. With our setup, we attempt to measure nitrogen-vacancy (NV) center spins of a diamond sample. This sample is advertised to have a low spin density (<5 ppb) [11].

For conducting reliable spin measurements, it is important to have a lower frequency uncertainty than the frequency shifts caused by spin interactions with the cantilever. This thesis aims to characterize the frequency noise of the setup. The influence of temperature, driving amplitude of the cantilever, and position on the frequency uncertainty will be discussed. It is also important to rule out any other causes of the frequency shift of the cantilever before concluding spin interactions. One effect that is expected to cause frequency shifts is the Meissner effect through the superconducting pickup loop. In this thesis, this effect is explored through a simulation and measurements.

1.1 Outline

In this thesis, chapter 2 discusses the theory necessary for the experiments conducted. Chapter 3 discusses the setup used for the experiment and the methodology. It also discusses a model made for simulating the frequency shift of the cantilever resulting from the Meissner effect. Chapter 4 shows the results of our measurements. Chapter 5 discusses these results and provides an outlook for further experiments. Finally, chapter 6 shows the conclusion of this thesis.

Version of August 1, 2025– Created August 1, 2025 - 13:51

Chapter 2

Theory

This chapter outlines the theoretical background relevant to this thesis. It will start with discussing the general theory of MRFM, followed by how this technique can be used to measure spins. Additionally, it will cover the Meissner effect, noise and frequency uncertainty in MRFM and the principles of detection using a lock-in amplifier.

2.1 Magnetic Resonance Force Microscopy

Magnetic Resonance Force Microscopy (MRFM) is a technique to measure external magnetic fields based on a change in the resonance frequency of a cantilever with a ferromagnetic particle placed on its tip.

The cantilever behaves like a harmonic oscillator and oscillates with a resonance frequency given by:

$$f_0 = \frac{1}{2\pi}\sqrt{\frac{k_0}{m}} \tag{2.1}$$

Here, f_0 is the resonance frequency of the harmonic oscillator in Hz, k_0 is the stiffness of the cantilever in N/m, and m is the mass of the cantilever. The ferromagnetic particle on the tip of the cantilever has a magnetic field $\vec{B_0}$, that at a distance r is equivalent to a dipole located at the center of this magnet. Thus, this magnetic field is given by [12]:

$$\vec{B_0}(\vec{r}) = \frac{\mu_0}{4\pi}[\frac{3\hat{r}(\hat{r}\cdot\vec{m}) - \vec{m}}{r^3}] \tag{2.2}$$

Here, $\mu_0 \approx 4\pi \cdot 10^{-7}\text{N/A}^2$ is the vacuum permeability constant, and $\vec{m}$ is the magnetic dipole moment of the magnetic particle in $\text{A} \cdot \text{m}^2$.
Two magnets exert a force on each other. Therefore, if there is another magnet in the presence of the cantilever, the cantilever experiences the following magnetic force:

$$\vec{F} = \nabla \left(\vec{m_{ext}} \cdot \vec{B_0} \right) \tag{2.3}$$

Here, $\vec{F}$ is the force that the magnet at the tip of the cantilever feels as a result of the external magnet in N and $\vec{m_{ext}}$ is the magnetic dipole moment from of external magnet in $\text{A} \cdot \text{m}^2$. This force influences the stiffness of the cantilever. Because the cantilever used in the experiment only has one degree of freedom, the x-direction, only the force in this direction influences the cantilever stiffness. From Hooke's law, we know that $F = -kx$. So, this change in stiffness k_s can be calculated through:

$$k_s = \frac{\partial F}{\partial x} = \vec{m_{ext}} \cdot \frac{\partial^2}{\partial x^2} \vec{B_0} \tag{2.4}$$

This change influences the resonance frequency of the cantilever, this change in resonance frequency can be calculated through [7]:

$$\Delta f = \frac{k_s}{2k_0} f_0 \tag{2.5}$$

2.2 Spin measurements

Spins have a magnetic moment [12], therefore they can be measured with MRFM. The magnetic moment of a spin μ_s is given by:

$$\mu_s = S\hbar\gamma \tag{2.6}$$

Here, S is the spin quantum number, $\hbar \approx 1.05 \cdot 10^{-34}\text{kg} \cdot \text{m}^2/\text{s}$ is the reduced Planck constant, and γ is the gyromagnetic ratio in $\text{A} \cdot \text{s/kg}$, which is a material-dependent constant. When spins experience an external magnetic field, they are either in a spin-up or a spin-down state. This means that the magnetic moment of the spins is either precisely in the same direction as the external magnetic field or in exactly the opposite direction [13]. These two spin states have an energy difference given by [14]:

$$\Delta E = 2\mu_s B_0 \tag{2.7}$$

Version of August 1, 2025– Created August 1, 2025 - 13:51

By sending a radio-frequency (RF) pulse with exactly this energy to the spin, its spin state can be changed. To accomplish this, the frequency of the radio-frequency pulse needs to be equal to the Lamor frequency of the spin, given by $\omega_L = \gamma|B_0|$ [14]. Because B_0 is dependent on the distance between the cantilever and the spin, the Lamor frequency is different for spins at different places in a material. This is why the frequency shift of the cantilever can be plotted as a function of the frequency of the RF pulse.

2.3 NV centers in diamond

The spins we are aiming to measure are from nitrogen-vacancy centers (NV centers) in diamond [15]. Diamond usually has a net spin of zero, but impurities like NV centers can cause a net spin in the sample [16]. The sample used in our experiment is advertised as having extremely low ($<$0.05 ppm) impurity levels [11]. This is desired because ideally, there should be no interactions between the spins in the material [7].

Nitrogen impurities are impurities where one of the ^{12}C atoms in a diamond lattice is replaced by a nitrogen atom. This nitrogen atom has one electron more than a carbon atom [16]. This electron is shared with other atoms in the lattice, and so a spin system will be formed [15]. If adjacent to the nitrogen atom, another carbon atom is missing, it is called an NV-impurity [16].

We can differentiate between two types of spins, bulk spins and surface spins. Because bulk spins have a longer relaxation time [15], they are easier to measure than surface spins. Therefore, our first goal is to measure the frequency shift of the cantilever due to interactions with bulk spins. A simulation of the frequency shift resulting from interactions between the cantilever and bulk spins, as a function of the frequency of the RF pulse used to manipulate these spins, was made by Loek van Everdingen. This simulation is shown in figure 2.1.

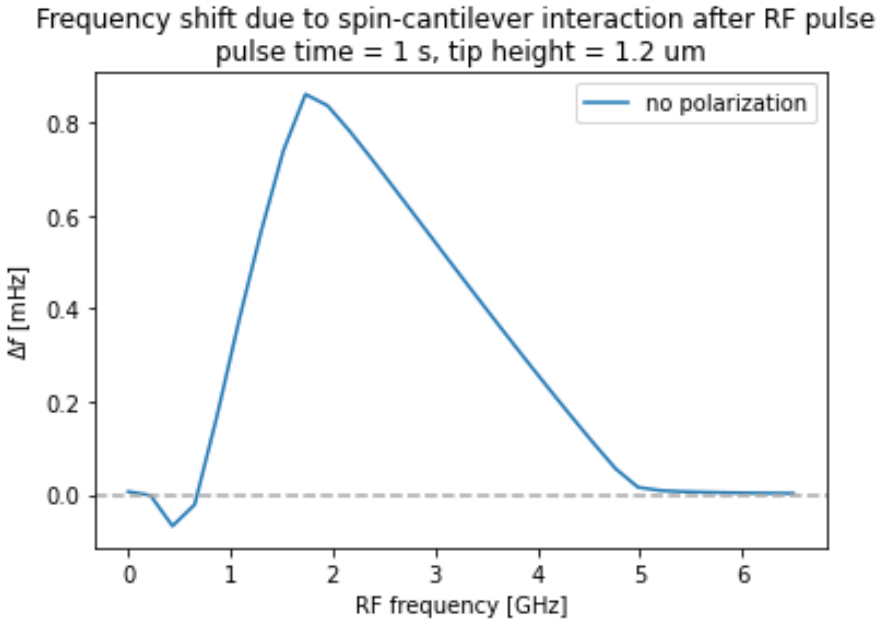

Figure 2.1: *A simulation of the expected frequency shift of the cantilever due to the interaction between the cantilever and bulk spins as a function of RF frequency. On the x-axis is the frequency of the RF pulse in GHz. On the y-axis is the frequency shift of the cantilever in mHz.*

2.4 Meissner effect

The Meissner effect [17] is an effect that occurs in superconducting materials. It prevents any net magnetic field from existing within the superconductor [18]. When certain materials are cooled below their critical temperature, they become superconducting. The thermal energy in the material is no longer high enough to oppose the very weak attractive force between electrons. The electrons will form pairs. These electron pairs behave like Bose particles instead of Fermi particles, which means that now all electrons can be in the same state [19].

Because all the electrons are in the same state, there is no electrical resistance. One of the consequences of this is that a magnetic field can not penetrate the metal when it is in the superconducting state. Because there is no electrical resistance in the superconducting material, a change of magnetic flux inside the material immediately produces an electric field. This electric field generates a current that, by Lenz's law, opposes the flux [18].

If a magnetic field penetrates a superconductor, the superconductor

will effectively generate a magnetic field opposing the original field. This magnetic field will also be felt outside of the superconductor [18]. In our experiment, we use a superconducting pickup loop, which becomes magnetized and induces a frequency shift in the cantilever.

2.5 Frequency noise and frequency uncertainty

In MRFM there are several sources of frequency noise, including mechanical noise, thermal noise, 1/f noise, instrumental noise, and deflection detector noise [20]. These frequency noise sources make it more difficult to measure small magnetic forces [14]. In this thesis we will discuss deflection detector noise and thermal noise.

2.5.1 Deflection detector noise

Deflection detector noise is a result of the the fact that the deflection of the cantilever can not be measured with infinite accuracy. This noise term is dominant when high measurement bandwidths are used. The deflection detector noise can be calculated through the following equation [21]:

$$\frac{\delta f_{det}}{f_0} = \sqrt{\frac{2}{3}} \frac{n_q BW^{\frac{3}{2}}}{A f_0} \tag{2.8}$$

Here, n_q is a constant that represents the accuracy with which the cantilever's deflection can be measured in $\mathrm{m}/\sqrt{\mathrm{Hz}}$. BW is the bandwidth used in the experiment in Hz, A is the amplitude of the cantilever oscillation in m, δf_{det} is the deflection detector frequency noise in Hz, and f_0 is the resonance frequency of the cantilever in Hz. We can thus see that, theoretically, the deflection detector noise increases with the measurement bandwidth and is inversely proportional to the amplitude of the cantilever.

2.5.2 Thermal noise

A fundamental limit to the frequency noise of the cantilever is given by its thermal noise. The higher the temperature of the cantilever, the more thermal energy it has. This causes thermal fluctuations of the cantilever position and frequency noise [14]. The thermal frequency noise can be calculated with the following equation [21]:

$$\frac{\delta f_{thermal}}{f_0} = \sqrt{\frac{k_B T B W}{\pi k A^2 f_0 Q}} \tag{2.9}$$

Here, $k_b \approx 1.38 \cdot 10^{-21}$ J/K is the Boltzmann constant, T is the temperature in K, k is the stiffness of the cantilever in N/m, and Q is the Quality factor of the cantilever oscillation. We see that the frequency noise of the cantilever increases with the square root of the temperature.

2.6 Lock-in amplifier

For conducting the measurements presented in this thesis, a Zurich Instruments lock-in amplifier was used. The information in this section about the detection principles of this device is based on a publication from Zurich Instruments [22].

A lock-in amplifier is an electrical instrument designed to extract the amplitude and phase of signals of interest from a noisy background signal. They can measure the amplitude and phase signals with the presence of noise peaks that have an amplitude up to ten million times higher than the desired signal. For this, a lock-in amplifier uses a homodyne detection scheme. This means that the lock-in performs a multiplication between the measured signal and its internal reference signal. This reference signal is often a sine wave. After performing the homodyne detection, the lock-in applies a low-pass filter to the signal so that the signal of interest can be extracted. This process is often referred to as demodulation.

2.6.1 Dual-phase demodulation

The amplitude and phase of a signal can be determined through dual-phase demodulation. Here, the input signal is split, then one part of the signal is multiplied by the reference signal, and one part is multiplied by the reference signal with a 90-degree phase shift. Then a low-pass filter is applied to these two signals, and they will have outputs X and Y as can be seen in figure 2.2.

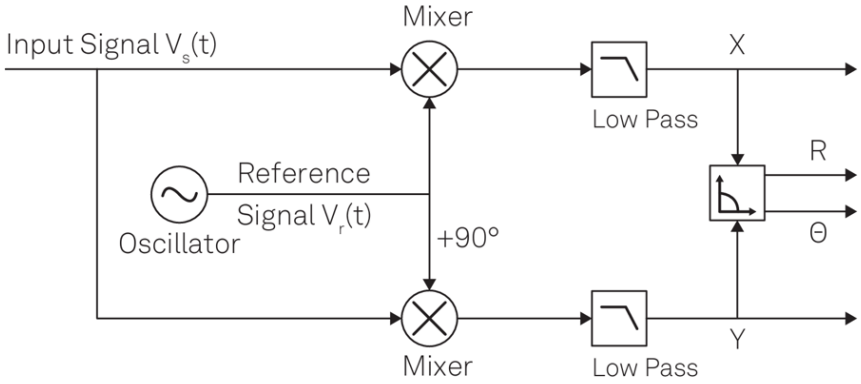

Figure 2.2: *A schematic representation of the lock-in amplification, using dual-phase demodulation. The input signal is split, then one part is multiplied by the reference signal, and one part is multiplied by a 90-degree phase-shifted version of the reference signal. A low-pass filter is applied to these outputs. Finally, the outputs are converted into polar coordinates. This figure has been reproduced from [22].*

From these X and Y, the amplitude (R) and phase (θ) of the signal can be determined through the following equations:

$$R = \sqrt{X^2 + Y^2} \tag{2.10}$$

$$\theta = atan2(Y, X) \tag{2.11}$$

2.6.2 Signal mixing in the frequency domain

Understanding signal mixing is easiest in the frequency domain. A signal can be transformed to the frequency domain with a Fourier transform. When a Fourier transform is applied to a sine wave, it will give two delta peaks, one at its frequency f_s and one at $-f_s$. For now, we will only take the positive peak into consideration. When a sine signal with frequency f_s is mixed with a reference signal f_r, the resulting signal will give two delta peaks in the frequency domain. One at frequency $f_s + f_r$ and one at frequency $f_s - f_r$. Often, the measured signal and reference signal are very close to each other. This will result in a peak at 0 Hz and a peak at $2f_s$. The 2 f_s peak will then be filtered out with a low-pass filter.

2.6.3 Phase-Locked Loop

A system that can be used to get f_s and f_r as close to each other as possible is a phase-locked loop (PLL). A PLL is a closed-loop feedback system that keeps a constant phase relation between two periodic signals. It works through a phase detector and a PID controller. The detector generates a signal that is proportional to the phase difference between the f_s and f_r signals. This signal is then sent through a PID controller that produces a feedback signal based on proportional, integral, and derivative operations on the error signal. For more information on the specific operations, see [23]. The feedback signal is then sent to a controlled oscillator. This oscillator, based on the feedback, generates a signal that follows the phase of the measured signal, thus generating a signal with the same frequency.

2.6.4 Choosing a low-pass filter

For directly isolating our signal, we would like to cut off all frequency signals above our desired signal. Unfortunately, such a filter does not exist. In reality, we can choose RC-filters of a certain order. These filters consist of a resistor with resistance R and a capacitor with capacitance C. The higher the order of the filter, the steeper the cut-off of the signal is. The signal with an n-th order RC-filter can be approximated by:

$$H_n(\omega) = (\frac{1}{1 + i\omega RC})^n \tag{2.12}$$

Here ω is the radial frequency of the signal, which can be calculated from f by $\omega = 2\pi f$.
However, the higher the order of a low-pass filter is, the more phase lag it will give in a signal, which might give problems when using the phase signal for giving feedback to a system, such as a PLL. Here, the additional phase lag will cause instability in the feedback system.
During the measurements, the bandwidth of the filter can be chosen. This choice is mainly a tradeoff between the signal-to-noise ratio (SNR), which is the ratio of the signal of interest to the noise in the measured signal, and the time resolution of the measurement. A lower bandwidth will lead to a higher SNR, but a lower time resolution.

Version of August 1, 2025– Created August 1, 2025 - 13:51

Chapter 3

Methods

This chapter presents the setup and methodology of the MRFM experiment. It starts with discussing the cryostat in which the experiment is conducted, followed by the MRFM setup. Then, the method for measuring the resonance frequency of the cantilever is given. After this, the positioning procedure of the cantilever is explained. Next, a way to measure phase and frequency uncertainty is discussed. The chapter concludes with a discussion of a possible model to simulate the frequency shift due to the Meissner effect due to the superconducting pickup loop used in the experiment.

3.1 Dilution fridge Marshmallow

The MRFM system used in this experiment is placed in a dry dilution refrigerator Marshmallow. A dry dilution refrigerator is a type of dilution refrigerator in which helium-4 is circulated through the cryostat by a pulse tube, this cools the cryostat down to around 4 K. The rest of the cooling is done by circulating a mixture of helium-3 and helium-4 through a mixing circuit. A dry dilution fridge usually has more vibrations than a dry dilution fridge, due to the varying pressure in the pulse tube. This varying pressure causes low-frequency square wave vibrations at the top of the cryostat. There are also vibrations in the kilohertz regime because of the higher harmonics from the gas flowing into the cryostat. For our MRFM system, these vibrations are countered by placing a mass-spring vibration isolation system between the mixing chamber plate of the cryostat and the MRFM system. This mass-spring system consists of a kHz damping system and damping for lower frequencies. For more information about this

system and other vibration isolation, see [24]. A picture of the cryostat can be seen in figure 3.1.

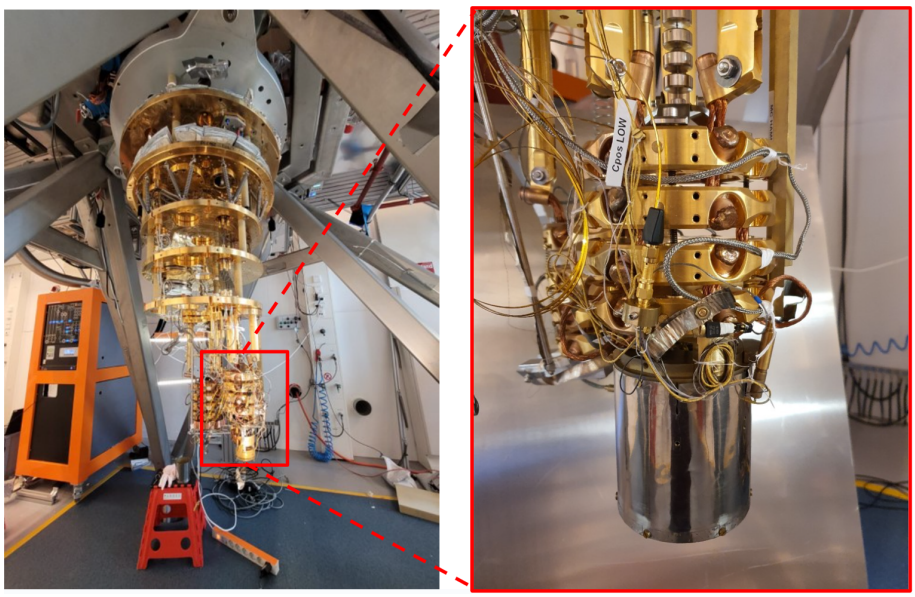

Figure 3.1: *On the left is a picture of the cryostat Marshmallow where our experiment was placed. On the right is a closer up picture of the experiment. This figure has been reproduced from [25].*

3.2 Setup

The MRFM system in Marshmallow is named the NV MRFM. The NV MRFM consists of a cylindrical copper sample holder and the cantilever and its positioning structure. The positioning system of the cantilever consists of a plate to which the cantilever is attached and 3 piezo knobs that can be extended to move the cantilever. The positioning system is explained in detail in section 3.5. In the middle of the sample holder, a detection chip is placed. A schematic representation of the setup is shown in figure 3.2.

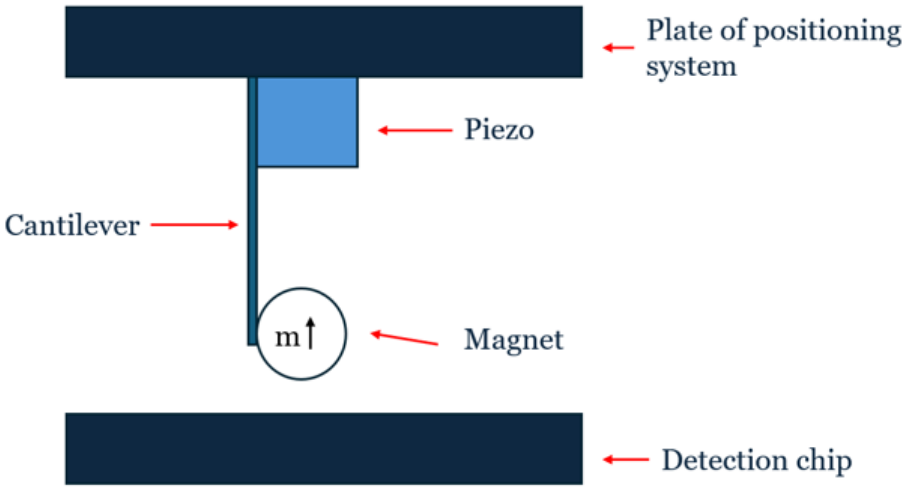

Figure 3.2: *A schematic representation of the MRFM setup. The cantilever is mounted on the plate of the positioning system with a piezo at its base. To the tip of the cantilever, a magnet with a magnetization in the z-direction is attached. The cantilever oscillates above the detection chip.*

3.2.1 Cantilever

The cantilever that is used in the experiment is an IBM-style silicon cantilever developed by Chui et al. [26] with a magnetic tip, a $Nd_2Fe_{14}B$ powder particle with a diameter of 3.4 μm [15], this particle is expected to have a remnant magnetization of 1.3 T [27]. This cantilever has a stiffness $k_0 \approx 7 \cdot 10^{-5}$ N/m and a resonance frequency $f_0 \approx 1.5 \cdot 10^3$ Hz. The cantilever has a length of 145 μm [15]. The cantilever can be electrically driven with a dither piezo that is attached to the base of the cantilever [7].

3.2.2 Detection chip

On the detection chip, a Diamond sample, a superconducting pickup loop, and RF cables are placed. The pickup loop is used to pick up the signal of the cantilever oscillation. This signal will go to a Superconducting Quantum Interference Device (SQUID). The RF cables will be used to send GHz pulses to manipulate spins in the diamond sample [7]. A picture of the detection chip can be seen in figure 3.3.

Version of August 1, 2025– Created August 1, 2025 - 13:51

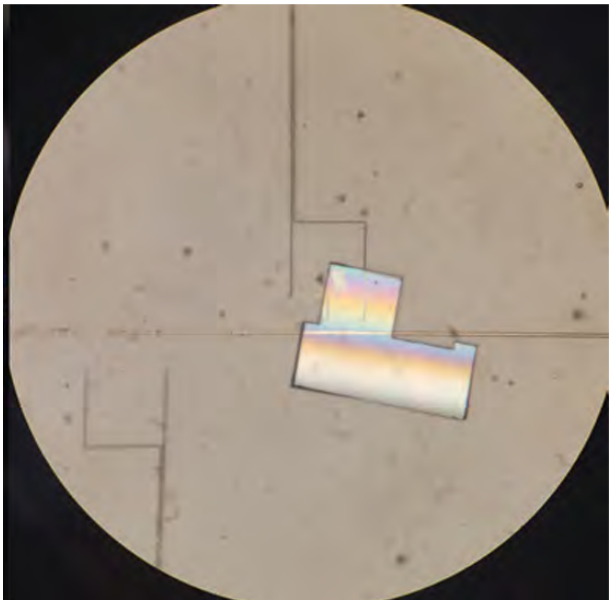

Figure 3.3: *A picture of the detection chip. On this chip, we see 2 pickup loops, a diamond sample, and in the middle, an RF line. This figure has been reproduced from [7].*

3.2.3 SQUID measurements

To detect the oscillation of the cantilever, we use a Superconducting Quantum Interference Device (SQUID). We do this by measuring the flux induced in a superconducting pickup loop by the cantilever tip. This pickup loop is coupled to the input coil of a SQUID. Using a SQUID makes it possible to do measurements below a temperature of 50 mK [14].

3.3 Frequency sweeps

One of the measurement techniques we use is a frequency sweep with a Zurich Instruments Lock-in amplifier. The detection principles of this device are described in section 2.6. A frequency sweep is a sweep where we use a piezo to drive the cantilever with different frequencies around its resonance frequency. We measure the amplitude and the phase of the cantilever signal at each frequency. The results of this sweep are a magnitude, phase, and polar plot. An example is shown in figure 3.4.

Version of August 1, 2025– Created August 1, 2025 - 13:51

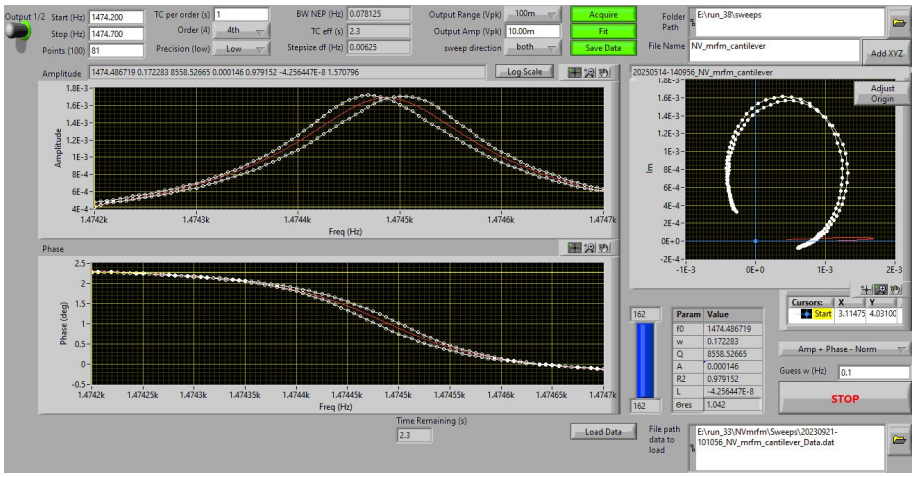

Figure 3.4: *An example sweep. At the top left, an amplitude plot of the frequency sweep is shown. Here, the x-axis shows the frequency in Hz, the y-axis shows the amplitude of the signal that the cantilever induces in the pickup loop in Volt. In red, a Lorentzian is fitted through all the data points. Below the amplitude plot, a phase plot is shown. Here, the x-axis is the frequency in Hz, the y-axis shows the phase of the cantilever signal. On the right, we see a polar plot, which is a combination of the amplitude and phase plot. We see that this plot forms a circle, which means that the plot is from a resonance.*

Each sweep is done over a frequency range of 0.5 Hz. During the sweep, the cantilever is driven both upward and downward in frequency. Because of nonlinearities in our system, the peaks do not exactly overlap. Through the amplitude plot, a Lorentzian is fitted. Through the phase plot, an arctangent function is fitted. From these fits, we can extract the resonance frequency of the cantilever f_0 and its amplitude at this frequency A. We also extract the Q-factor Q of the resonance, which is the width of the peak at half maximum.

3.4 Cantilever coupling

To perform our experiment, the cantilever must be positioned near the pickup loop in a location with strong coupling, where its oscillations can be effectively detected. As a measure of the coupling, we use the amplitude of the oscillation from the cantilever A/Q.

Because the actual size of A and Q we get out of the sweep depends on multiple things besides the coupling, A/Q is only used to compare the coupling at different positions, not as an actual quantity.

3.5 Positioning of the cantilever

This section will describe the positioning system of the cantilever, the positioning readout, and the positioning procedure used in this thesis.

3.5.1 Positioning system

To find the ideal coupling of the cantilever, we have to 'walk' with it. We do this using three Piezo knobs, that are all attached to a plate to which the cantilever is attached. A 2D sketch of this system can be seen in figure 3.5.

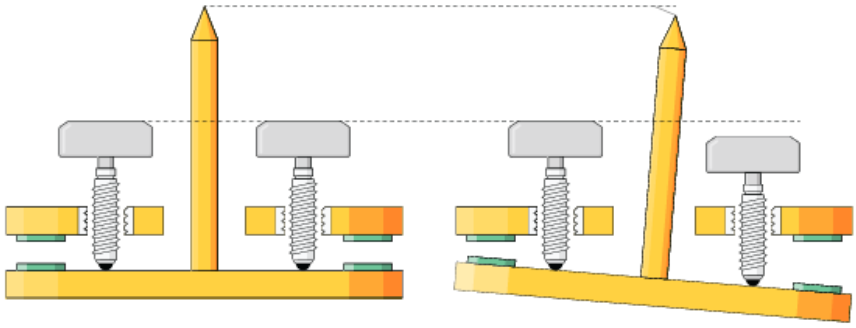

Figure 3.5: *A 2D sketch of the positioning system used in the NV MRFM. If one of the knobs is extended, the plate to which the cantilever is attached will tilt. This moves the position of the cantilever. The green disks represent capacitor plates that are used for the position readout. This figure has been reproduced from [7].*

The piezo knobs can all be extended separately, if all three of the knobs are extended the same amount, the plate moves downwards towards the sample. If one or two of the knobs are extended, the plate tilts a bit so that the cantilever moves in the x, y, and z direction at the same time [7]. The piezo knobs are stick-slip motors, which means that the movements in x, y and z are not fluent. Instead, the movements are in small 'shocks', all with a slightly different efficiency. This makes it harder to walk straight in a certain direction.

3.5.2 Position readout

The x-, y-, and z-positions are calculated based on three sets of capacitor plates. One of these sets is placed next to each motor, as shown in figure 3.5. The capacitance between each of the pairs is inversely proportional to

the distance between the plates, so with a combination of the three capacitance values, the position of the cantilever can be determined [15].

3.5.3 Positioning procedure

At each cantilever position, we perform a frequency sweep. When positioning, we attempt to walk in a single cartesian direction, for instance the y-direction. We compare the resulting variation in the parameter A/Q to models that were developed in our group to calculate the coupling [15]. An example of an x-slice and a y-slice of this simulation are shown in figure 3.6 and figure 3.7.

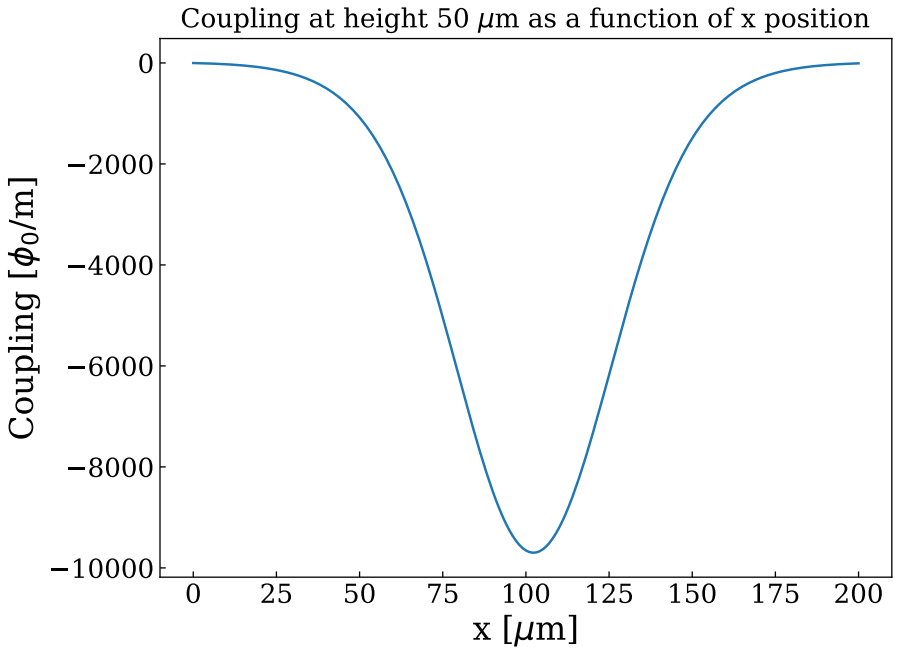

Figure 3.6: *Example slice of the simulation of the coupling at a height of 50 μm above the sample as a function of x-position. On the x-axis is the x-position in μm. On the y-axis is the coupling in ϕ_0/m.*

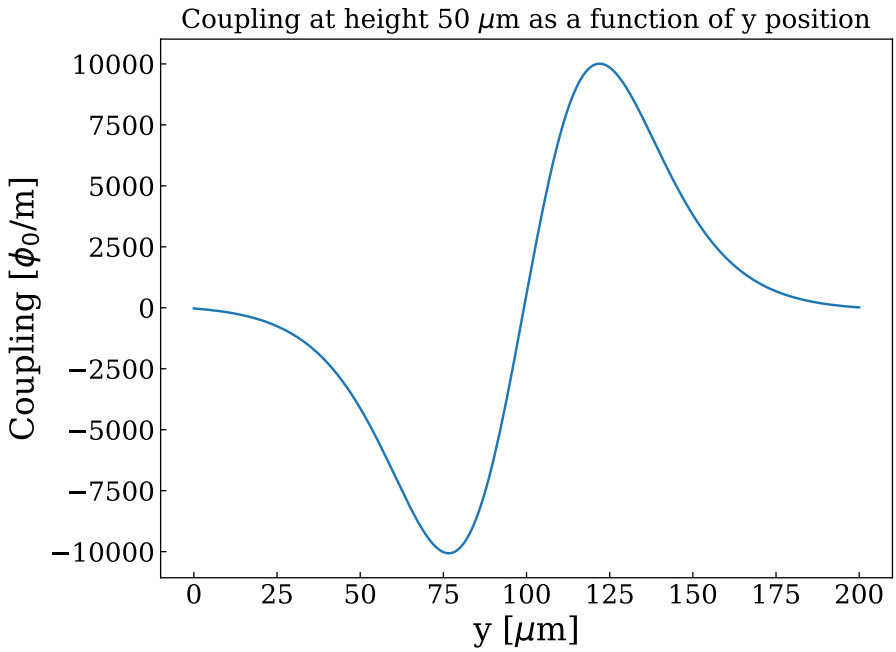

Figure 3.7: *Example slice of the simulation of the coupling at a height of 50 μm above the sample as a function of y-position. On the x-axis is the y-position in μm. On the y-axis is the coupling in ϕ_0/m.*

Because in the simulation, the place of the pickup loop and diamond sample are known. We can use these simulations to calculate these positions in terms of the coordinate system of the capacitor plates, by using the offset between the simulated and the measured coupling curves. This is necessary because each time the cantilever is cooled down to low temperatures, this coordinate system changes, due to contraction of setup materials during the cool down [14]. We can also use the broadness of the A/Q curve to determine the height of the cantilever above the sample, as a broader A/Q curve means a bigger distance between the cantilever and the pickup loop.

3.5.4 Unit conversion

The A/Q parameter we get from a frequency sweep can be converted to the units used in the simulation from Marc de Voogd [15]. We can use this conversion to see if the coupling is as high as expected. If the coupling is not as high as expected, this could indicate a defect of one of the components of our setup. The unit used in this simulation is $\frac{\mu\phi_0}{nm}$. The frequency

sweep gives A/Q in Volt. To convert these units, we use the following equation:

$$\frac{A_{simulation}}{Q_{simulation}} = \frac{A_{sweep}}{Q_{sweep} \cdot \eta \cdot V \cdot k} \tag{3.1}$$

For this calculation, we use the transfer coefficient from the SQUID k, which is $4.6 \cdot 10^3 \ \frac{\mu V}{\phi_0} = 4.6 \cdot 10^{-3} \frac{V}{\phi_0}$and the piezo response η, which is $40\frac{nm}{V} = 40 \cdot 10^{-9} \frac{m}{V}$. Here, $\frac{A_{sweep}}{Q_{sweep}}$ is in Volt, $\frac{A_{simultaion}}{Q_{simulation}}$ is in $\frac{\phi_0}{m}$, and V is the driving voltage of the cantilever is in Volt.

3.6 Frequency uncertainty measurements

To have a successful spin measurement, we need to make sure that our frequency uncertainty is smaller than the frequency shifts that are caused by spin interactions. We measure uncertainty in our cantilever frequency by using the phase-lock loop (PLL) from a Zurich instrument lock-in amplifier. The working principles of the PLL are explained in section 2.6.3. Our uncertainty measurements were performed with a PLL bandwidth of 3.405 Hz.

3.6.1 Frequency uncertainty as a function of temperature

In section 2.5.2 is stated that theoretically, the frequency noise in an MRFM system depends on the temperature of the experiment. To measure how the frequency uncertainty of our cantilever depends on the temperature of our experiment, we use a temperature PID made by Wim Bosch [28]. This PID system works by sending power to 2 heaters placed close to our MRFM system, based on the current temperature and desired temperature. By doing this, we can get a very constant temperature during our measurement.

For our measurements, we chose a place close to the pickup loop, approximately 1 μm above where we expect the surface to be. For each of the chosen temperatures, we set the center frequency of our PLL such that our signal has the highest amplitude possible. We then measure the frequency and phase of our signal during one minute.

Because section 2.5.1 shows that theoretically the frequency noise of the cantilever does depend on the cantilever amplitude, we do this for a total of 9 driving voltages per temperature. We can calculate the frequency uncertainty from the phase uncertainty by using the phase plot of

a frequency sweep. This can be done by looking at the slope of the phase plot. An example is shown in figure 3.8.

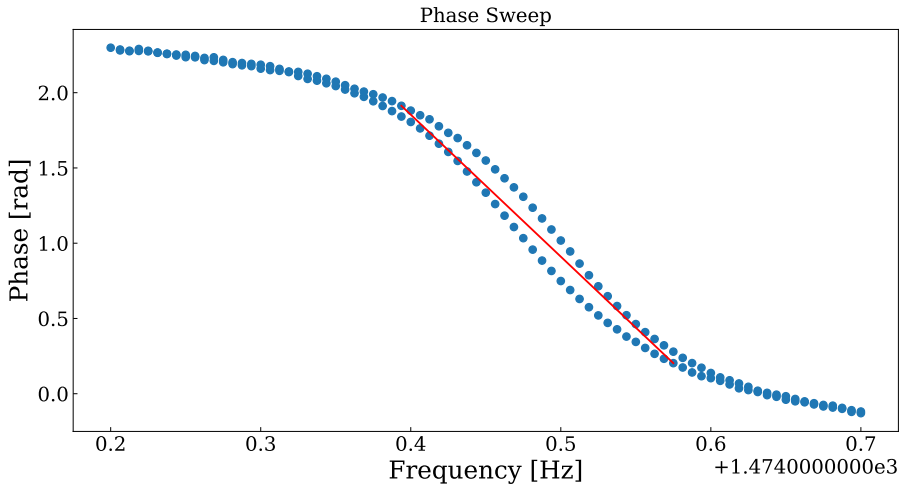

Figure 3.8: *An example sweep for determining the slope of the phase plot. The x-axis is the frequency in Hz. The y-axis is the phase of the cantilever signal in rad. In red, a line is drawn to determine the slope of the phase plot. We can use this slope to calculate the frequency from the phase data.*

In this example, the slope is $\frac{98^\circ}{0.18Hz}$, so in this case a phase uncertainty of 1° is consistent with a frequency uncertainty of $\frac{0.18}{98} = 1.8 \cdot 10^{-3}$ Hz.

3.6.2 Frequency uncertainty as a function of position

While testing the measurements described in the previous section, we observed that the frequency uncertainty of the cantilever varied with its position. We decided to explore this further and measure the frequency uncertainty as a function of the y-position of the cantilever. We chose 6 different y-positions while keeping the x- and z-position as constant as possible. For each of the chosen positions, we again set the center frequency of our PLL such that our signal has the highest amplitude possible. During these measurements, we also set a phase setpoint. We again measured for one minute. This time, we chose three different driving voltages.

3.7 Simulation Meissner effect

In our experiment, the magnet at the tip of the cantilever causes the superconducting pickup loop to generate its own magnetic field. This extra

magnetic field causes a shift in the resonance frequency of the cantilever. To get an estimation of the amount of frequency shift we can expect, we make a simulation where the frequency shift of the cantilever is shown at different positions. For this simulation, we assume that each part of our pickup loop can be seen as a row of mirror dipoles that perfectly oppose the magnetic field of the cantilever at their respective positions. If we follow this model, we can calculate the frequency shift in the following way. First, we use equation 2.2 to calculate the magnetic field from the cantilever at the place of the pickup loop.

For $\vec{m}$ we use the magnetic moment of the cantilever tip. In our case, this is given by:

$$\vec{m} = [0, 0, \frac{4\pi}{3}\frac{R^3 RMT}{\mu_0}] \tag{3.2}$$

In this equation, RMT_{tip} is the remnant magnetization of the cantilever-tip. In our case, this is 1.3 T [27]. R is the radius of the cantilever tip.

To find the magnetic field from the superconducting pickup loop at the position of the cantilever, we again fill in equation 2.2, but now we have $\vec{m}$ in the $-\hat{z}$-direction, for RMT we fill in the magnetic field from the cantilever at the place of the loop, and for R we fill in the radius of a dipole that is used for the simulation. We can then calculate the force between the loop and the cantilever with equation 2.3. With this force we calculate the frequency shift of the cantilever through equations 2.4 and 2.5. An example of a slice of this simulation can be seen in figure 3.9.

Version of August 1, 2025– Created August 1, 2025 - 13:51

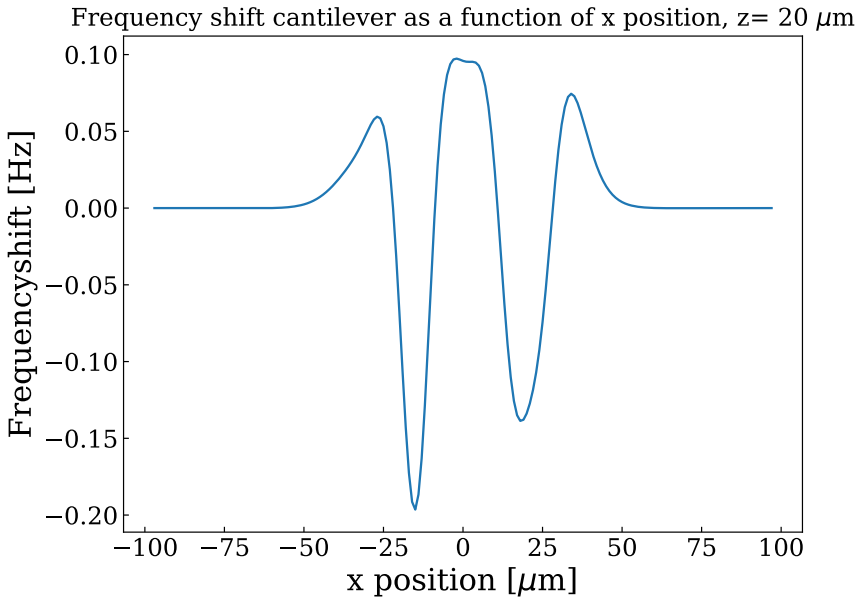

Figure 3.9: *A slice of the simulation of the expected frequency shift of the cantilever at z=20 μm as a function of x-position. On the x-axis is the x-position in μm. On the y-axis is the frequency shift of the cantilever in Hz.*

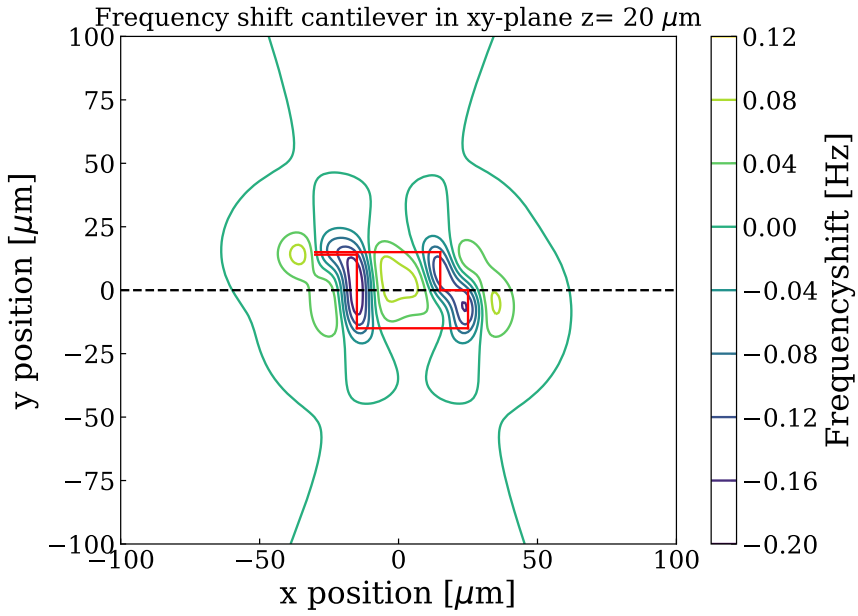

Figure 3.10: *A xy plane of the simulation of the expected frequency shift of the cantilever at z=20 μm. On the x-axis is the x-position in μm. On the y-axis is the y-position in μm. The black line shows the place of figure 3.9 is.*

Chapter 4

Results

In this chapter, the results of our measurements are shown. First, the positioning is discussed. With the measured coupling, the efficiency of the piezo is calculated. After this, frequency uncertainties in our setup are shown as a function of driving amplitude of the cantilever, temperature, and y-position. The chapter concludes by attempting to verify the model of the Meissner effect discussed in section 3.7 using the resonance frequencies obtained from the other measurements.

4.1 Positioning

Before conducting our measurements, it is important to know the position of the cantilever relative to the pickup loop and the diamond sample. We can calculate this position by converting the x,y and z coordinates of the cantilever from the coordinate system of the capacitor plates into the coordinates used in the simulation of Marc de Voogd [15]. In this coordinate system, the positions of the pickup loop and diamond sample are known. To find a way to convert the coordinate system of our capacitor plates to that of the simulation, we do a full x-sweep with constant y-position, and a full y-sweep with a constant x-position, where we measure A/Q at every position. Then we find an x-slice and a y-slice of the simulation that have a similar shape. At each height above the sample, the simulation curve has a different broadness. If we compare the broadness of our measured A/Q curve with x-sweeps and y-sweeps from the simulation at different heights, we get an idea of the cantilever height above the sample. We chose to use our y-sweep for this as its curve has an up and a down part, so it's easier to overlap precisely.

Because the units in our sweep are not the same as the units from the simulation, we have added a scaling factor to the simulation curve. We also added an offset so the measured positions coincided with the simulated positions. We did not have to change the y-scale as both of them are in μm. We can see the results from this sweep in figure 4.1 and figure 4.2.

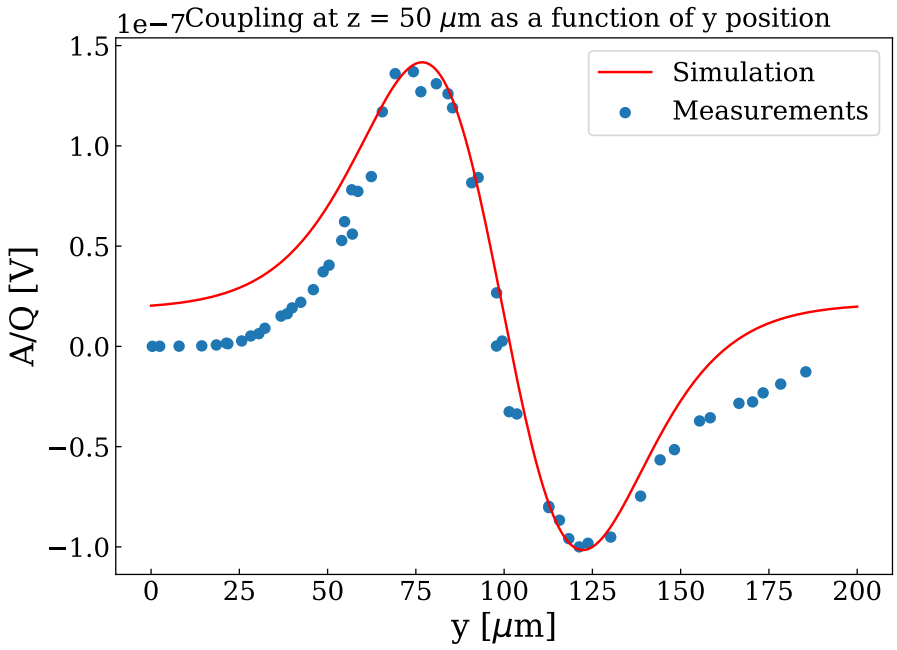

Figure 4.1: *Coupling as a function of y-position. The blue dots represent the measured A/Q, the red line represents the simulation of the cantilever coupling at a height of 50 μm above the sample. On the x-axis is the y-position in μm in the coordinate system of the simulation. An offset was added to the y-positions of the measured curve so they coincide with the y-positions of the simulation. On the y-axis is A/Q in V. A scaling factor was added to the simulation so it overlaps with the measured curve. We can see that the measured curve is a bit smaller than the curve of the simulation.*

Version of August 1, 2025– Created August 1, 2025 - 13:51

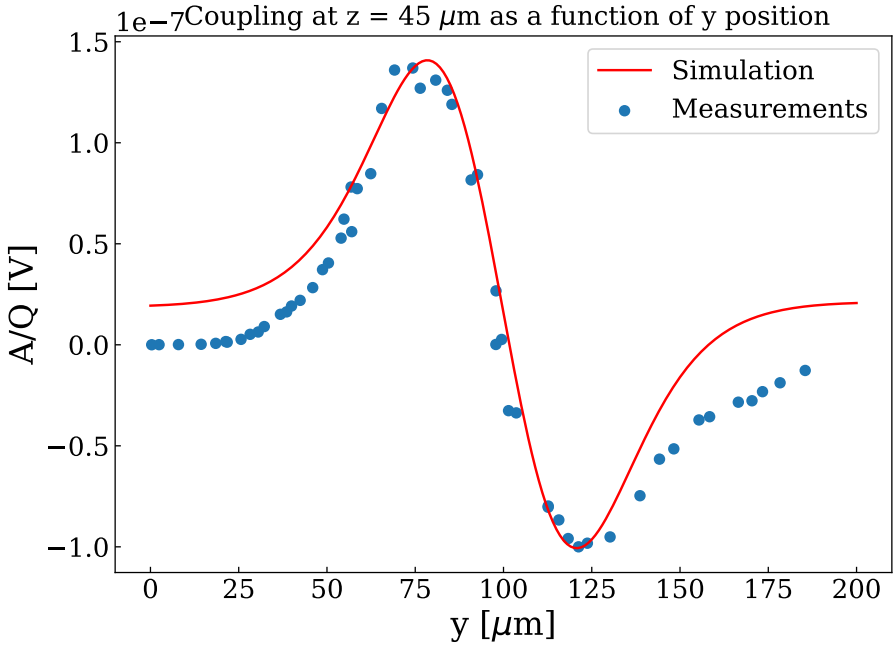

Figure 4.2: *Coupling as a function of y-position. The blue dots represent the measured A/Q, the red line represents the simulation of the cantilever coupling at a height of 45 μm above the sample. On the x-axis is the y-position in μm in the coordinate system of the simulation. An offset was added to the y-positions of the measured curve so they coincide with the y-positions of the simulation. On the y-axis is A/Q in V. A scaling factor was added to the simulation so it overlaps with the measured curve. We can see that the measured curve is a bit broader than the curve of the simulation.*

In figure 4.1, we see that the measured peak of the cantilever coupling is a bit smaller than the simulated cantilever coupling at a height of 50 μm above the sample. In figure 4.2 we see that the measured peak of the cantilever coupling is a bit broader than the simulated cantilever coupling at a height of 45 μm above the sample. This indicates that the shape of the A/Q curve of the current z of the motor coordinate system, which is around 620 to 622 μm, is most similar to the simulated curve corresponding to a height between the 45 and 50 μm above the sample.

When the conversion for the z-position from the coordinate system of the capacitor plates to the coordinate system of the simulation is found, the simulation curves at this height can be used to determine the x- and y-offsets between the two coordinate systems. For the y-position, this can be done by using figure 4.1, but removing the offset in y-position, this result can be seen in figure 4.3.

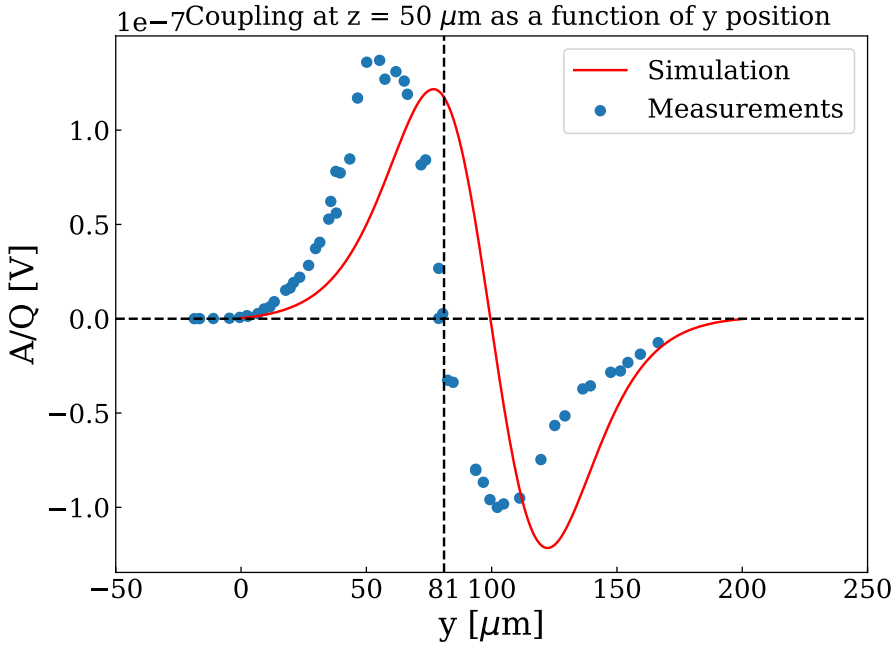

Figure 4.3: *Coupling as a function of y-position. The blue dots represent the measured A/Q, the red line represents the simulation of the cantilever coupling at a height of 50 μm above the sample. On the x-axis is the y- position in μm, now there is no offset of the y-position of the measured curve to fit the simulation. On the y-axis is A/Q in V. A scaling factor was added to the simulation so that its amplitude is similar to that of the measured curve. We see that the curves have the same shape, but lie 19 μm from each other,*

We see that the curve from the measurements and the curve from the simulation differ by about 19 μm from each other. The same can be done for the x-position. In figure 4.4 we see that the x-curves differ by 158 μm.

Version of August 1, 2025– Created August 1, 2025 - 13:51

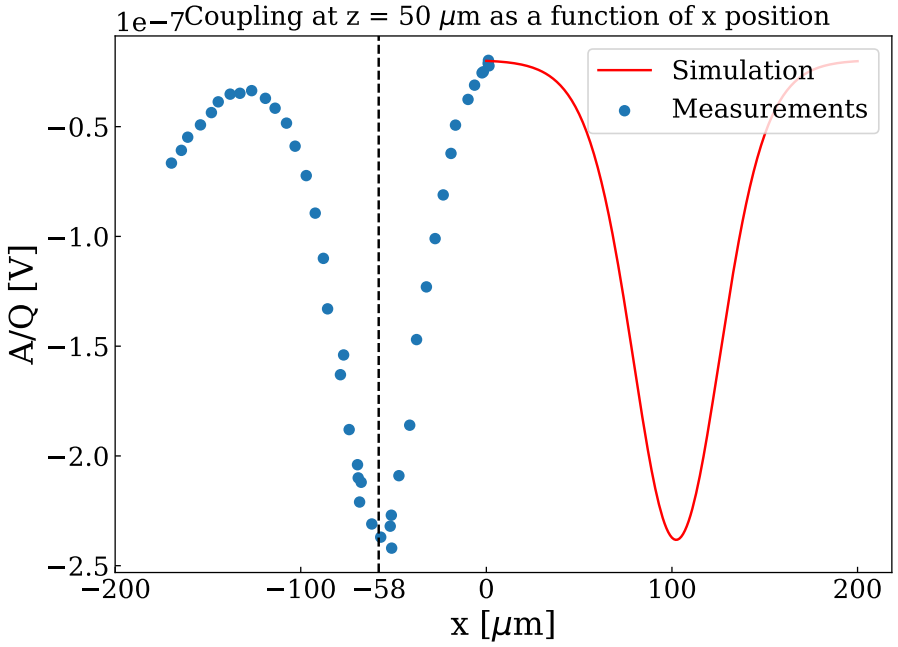

Figure 4.4: *Coupling as a function of x-position. The blue dots represent the measured A/Q, the red line represents the simulation of the cantilever coupling at a height of 50 μm above the sample. On the x-axis is the x-position in μm. On the y-axis is A/Q in V. A scaling factor was added to the simulation so that its amplitude is similar to that of the measured curve. We see that the curves have the same shape, but lie 158 μm from each other.*

4.1.1 Coupling

During the measurements, concerns arose that the coupling between the cantilever and the pickup loop was systematically worse than expected. This could indicate that the piezo for driving the cantilever was defective. To see if this was the case, we used equation 3.1 to convert the units of our measurements. The result of this calculation is shown in figure 4.5.

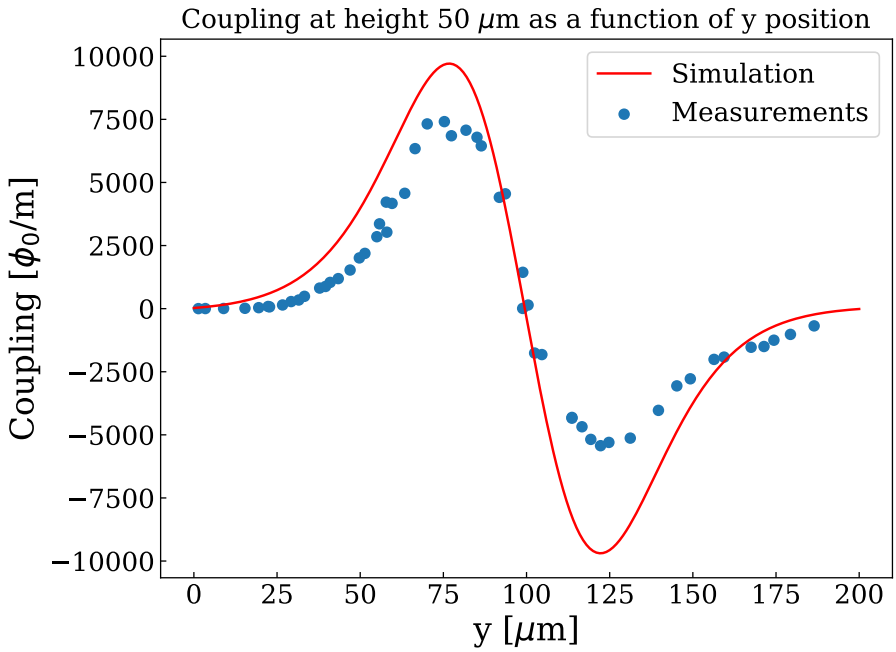

Figure 4.5: *Coupling as a function of y-position. The blue dots represent the measured A/Q, the red line represents the simulation of the cantilever coupling at a height of 50 μm above the sample. On the x-axis is the y-position in μm in the coordinate system of the simulation. An offset was added to the y-positions of the measured curve so they coincide with the y-positions of the simulation. On the y-axis is A/Q in ϕ_0/m. We see that the amplitude of the measured curve is of the same order of magnitude as that of the simulated curve.*

Figure 4.5 shows that the measured coupling is of the same order of magnitude as the expected coupling. When comparing the highest coupling measured to the coupling at the same y-position in the simulation, we find an efficiency of 76.3%.

4.2 Frequency uncertainty

Before we are able to measure spins, we need to make sure the uncertainty in our measurements is lower than the signal we expect to measure from due to spin interactions. Therefore, we characterized the frequency uncertainty of our measurements as a function of a few different parameters that could influence this uncertainty: the driving amplitude of the cantilever, the temperature of the experiment, and the position of the cantilever. For each measurement, the phase uncertainty of the cantilever was measured

Version of August 1, 2025– Created August 1, 2025 - 13:51

using a phase-locked loop. These phase uncertainties were converted to frequency uncertainties with the method shown in section 3.6.1.

4.2.1 Temperature and driving voltage dependence of frequency uncertainty

We measured the uncertainty of the cantilever for different driving voltages at different temperatures. The results of these measurements are shown in figure 4.6.

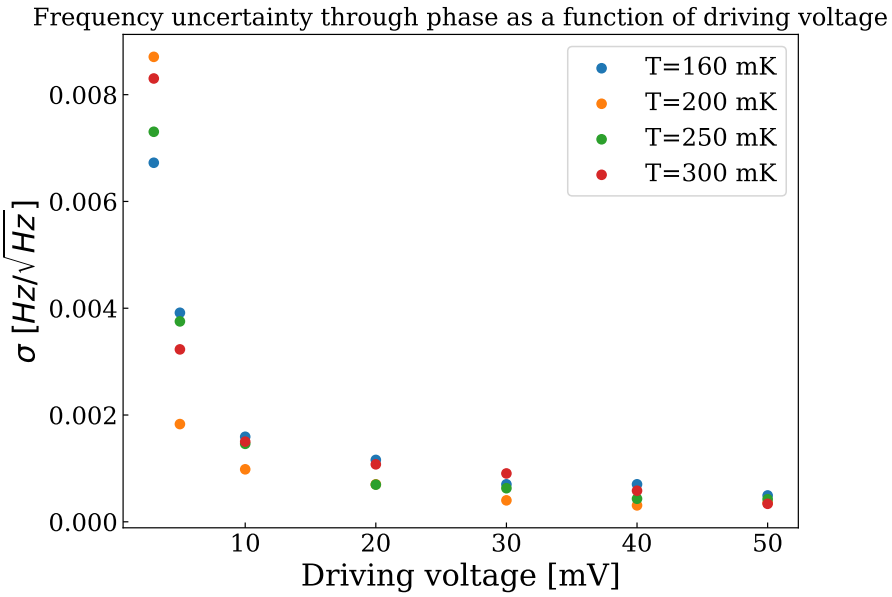

Figure 4.6: *Frequency uncertainty of the cantilever as a function of driving voltage for different temperatures. On the x-axis is the driving voltage in mV, on the y-axis the sigma of the frequency uncertainty of the cantilever in $Hz/\sqrt{Hz}$. We see that the frequency uncertainty decreases when the driving voltage increases. We see no clear trend in temperature dependence.*

Figure 4.6 shows that the frequency uncertainty of the cantilever decreases as the driving voltage of the cantilever increases. It is also shown that there seems to be no clear trend in the temperature dependence.
In section 2.5.1, equation 2.8 showed that the deflection detector noise is inversely proportional to the cantilever amplitude. As mentioned in section 3.5, we assume a linear relation between the driving amplitude of the cantilever and the amplitude of the cantilever oscillation. Therefore, we

Version of August 1, 2025– Created August 1, 2025 - 13:51

used the scipy curve fit function to fit the following equation to our measurements:

$$y = \frac{a}{x} \tag{4.1}$$

This fit is shown in figure 4.7.

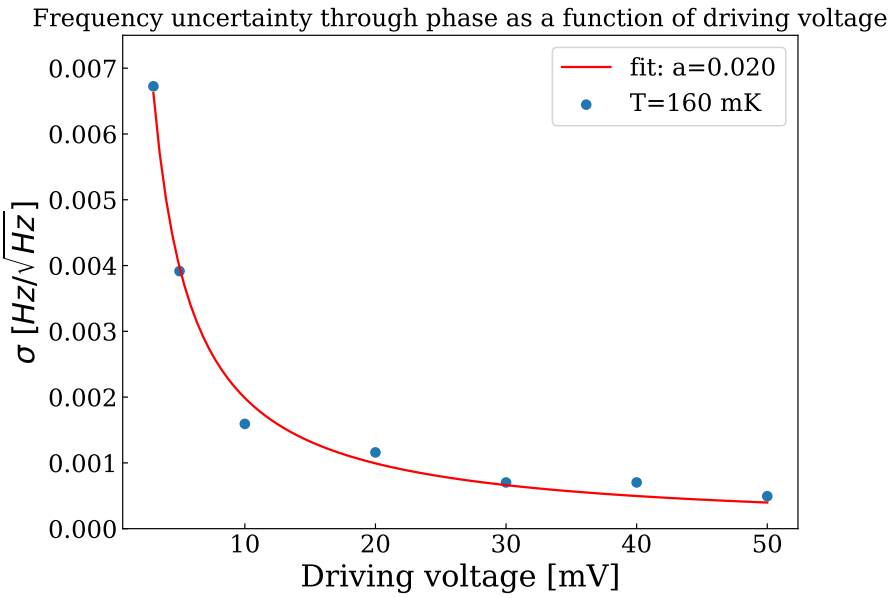

Figure 4.7: *Frequency uncertainty of the cantilever as a function of driving voltage with an a/x fit. On the x-axis is the driving voltage in mV, on the y-axis the sigma of the frequency uncertainty of the cantilever in $Hz/\sqrt{Hz}$.*

The value for a that was acquired from fitting the function to the data measured at a temperature of 160 mK is $a = (1.99 \pm 0.05) \cdot 10^{-2}$ and the fit has a root mean squared error (RMSE) of $1.8 \cdot 10^{-4}$. The fit was also made for the measurement at the other temperatures. The results of all the fits are given in table 4.1.

Temperature [mK]	a	RMSE
160	$(1.99 \pm 0.05) \cdot 10^{-2}$	$1.8 \cdot 10^{-4}$
200	$(2.1 \pm 0.3) \cdot 10^{-2}$	$1.2 \cdot 10^{-3}$
250	$(2.06 \pm 0.09) \cdot 10^{-2}$	$3.4 \cdot 10^{-4}$
300	$(2.2 \pm 0.2) \cdot 10^{-2}$	$6.3 \cdot 10^{-4}$

Table 4.1: *Results of the a/x fit to the frequency uncertainty as a function of driving amplitude.*

We see that the values for a are similar for each fit.

4.2.2 Position dependence of frequency uncertainty

While testing the measurements shown in section 4.2.1, we noticed that the frequency uncertainty was different at different cantilever positions. Therefore, we chose to measure the uncertainty at different y-positions close to the pickup loop, while keeping the x- and z-position as constant as possible. All the y-positions in this section are in μm, and are in the coordinate system of the capacitor plates.

Version of August 1, 2025– Created August 1, 2025 - 13:51

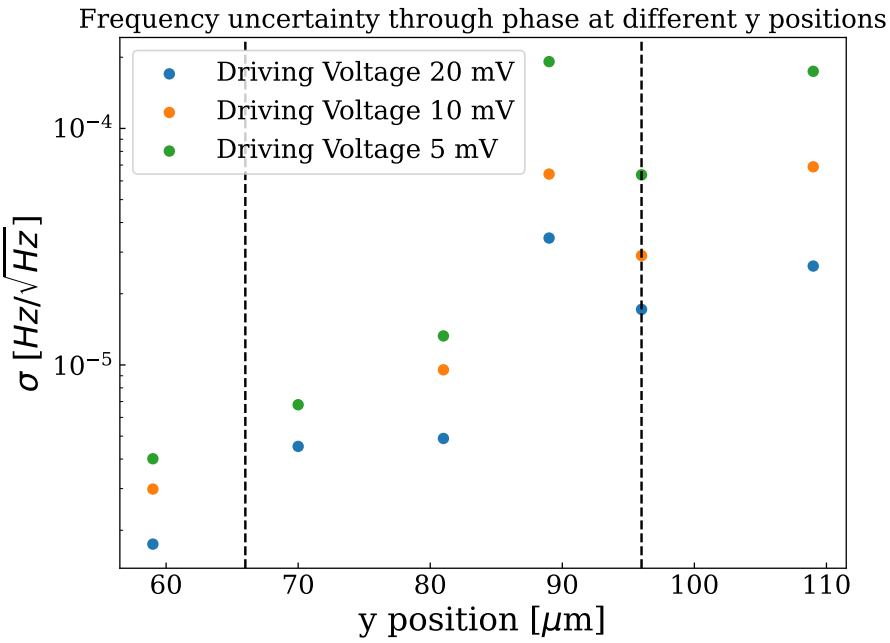

Figure 4.8: *Frequency uncertainty of the cantilever as a function of y-position for different driving voltages. On the x-axis is the y-position in μm, on the y-axis the sigma of the frequency uncertainty of the cantilever in $Hz/\sqrt{Hz}$ on a logarithmic scale. The black dashed lines show the lines of the pickup loop. We see that the frequency uncertainty increases towards the positive y-position.*

Figure 4.8 shows that the frequency uncertainty increases towards the positive y-position. We also observe an outlier at y = 89 μm.

4.2.3 Frequency noise spectra

From the frequency data at the different y-positions, frequency noise spectra were created. If we take the Fourier transform of the frequency data, we obtain a noise spectrum. This allows us to observe the amount of noise at a given absolute frequency relative to the resonance frequency. The results from this analysis are shown in figure 4.9. This figure shows that the curves of the noise spectra lie higher at a more positive y-position for the first 30 Hz from the resonance frequency. With the exception being y= 89 μm. After 30 Hz, we see that the noise spectra at 59 at 70 μm form a plateau.

Version of August 1, 2025– Created August 1, 2025 - 13:51

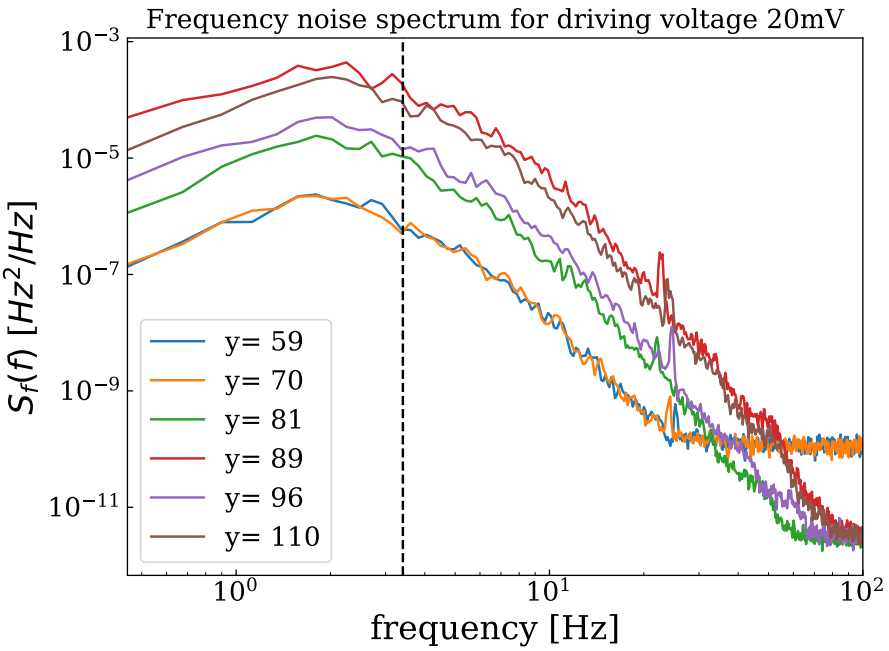

Figure 4.9: *Frequency noise spectrum of the cantilever with a PLL around its resonance frequency for different y-positions. During these measurements, the cantilever was driven with a driving voltage of 20 mV. On the x-axis is the absolute frequency relative to the resonance frequency in Hz. On the y-axis is the noise power in Hz^2/Hz on a logarithmic scale. The black vertical line gives the bandwidth of the lock-in used in the experiment, 3,405 Hz. We see that the frequency noise spectrum is higher for more positive y-positions.*

We also compared the frequency noise spectra with different driving voltages at the same position. For y= 81 μm the results can be seen in figure 4.10. This figure shows that the noise spectrum lies higher for a lower driving voltage.

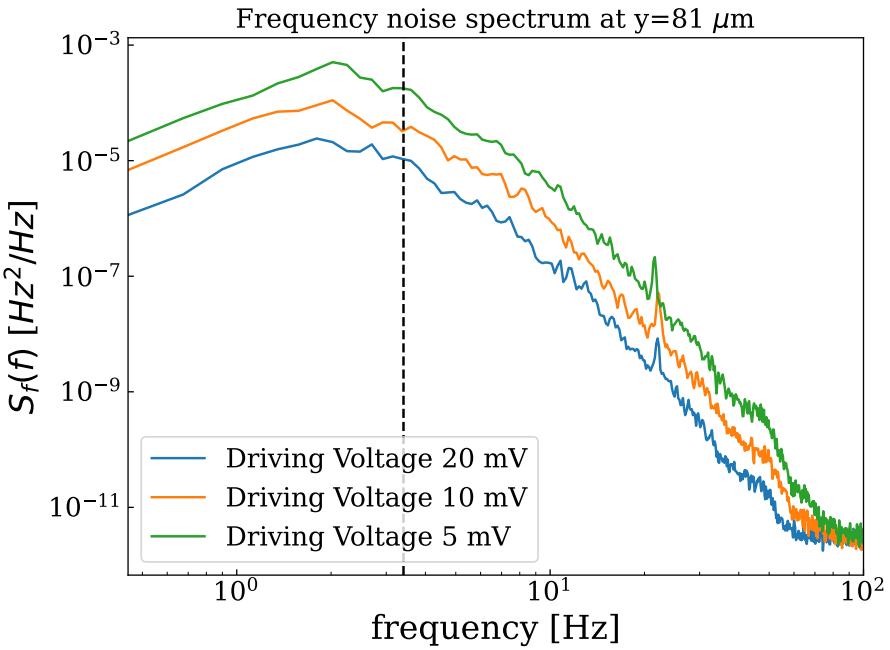

Figure 4.10: *Frequency noise spectrum of the cantilever with a PLL around its resonance frequency at y= 81 μm for different driving voltages. On the x-axis is the absolute frequency relative to the resonance frequency in Hz. On the y-axis is the noise power in Hz^2/Hz on a logarithmic scale. The black vertical line gives the bandwidth of the lock-in used in the experiment, 3,405 Hz. We see that the frequency noise spectrum is higher for a lower driving voltage.*

4.3 The Meissner Effect

Spins are not the only cause of cantilever frequency shifts. An example of another cause of a shift in the cantilever's resonance frequency is Meissner effect. This effect causes the superconducting pickup loop used in the measurements to become magnetized, thus causing a frequency shift of the cantilever. To estimate how much frequency shift this effect would cause, a simulation was created. This simulation was explained in section 3.7. To see if this model gives an accurate representation, the model was compared to the resonance frequencies of the cantilever at the different y-positions from section 4.2 and during the y-sweep described in section 4.1. In this section, we used the results from section 3.5 to add an offset to the measured y-positions so they would coincide with the coordinate system used in the simulation.

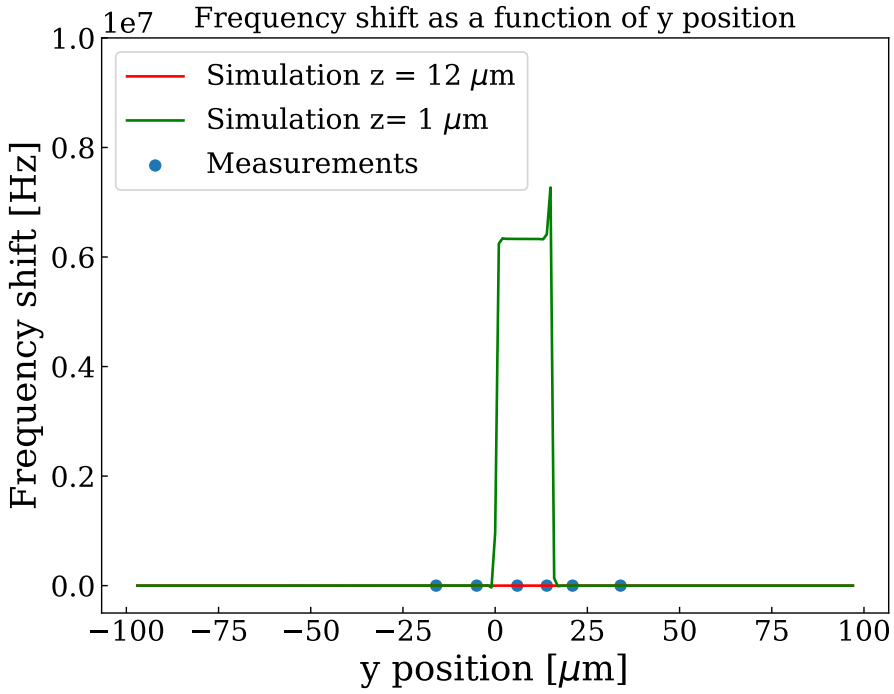

Figure 4.11: *The frequency shift of the cantilever at z=1 μm as a function of y-position compared to different simulation slices from the simulation of the frequency shift caused by the Meissner effect. On the x-axis is the y-position in μm. On the y-axis is the frequency shift of the cantilever in Hz. The green line shows the frequency shift of the cantilever predicted by the simulation at the height of the actual measurements. We see that the simulation shows a higher frequency shift than the frequency shift that was measured. The red line shows the best-fit simulation slice, which is from the simulation at a height of 12 μm.*

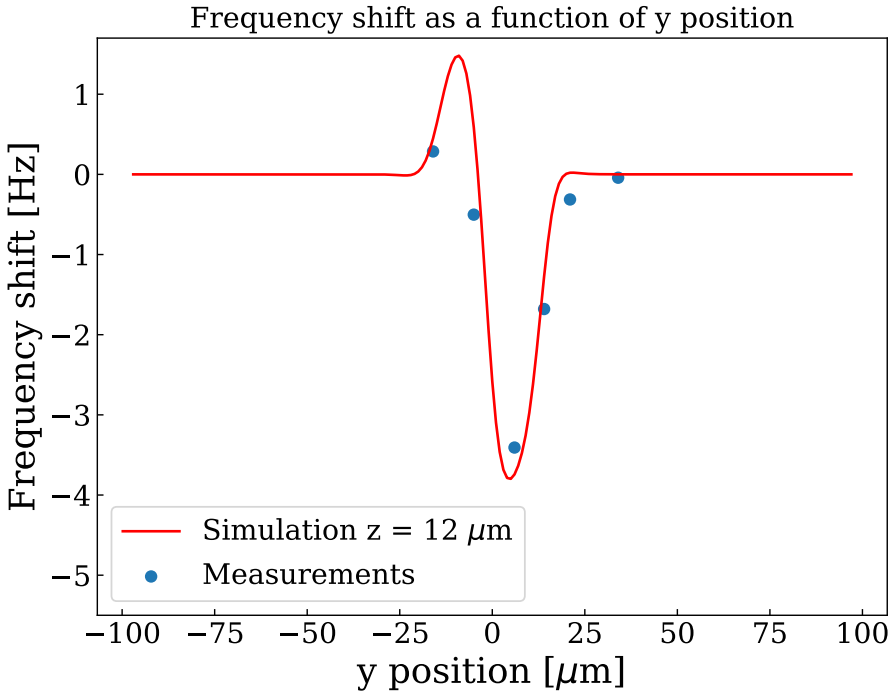

Figure 4.12: *The frequency shift of the cantilever at z=1 μm as a function of y-position compared to a best-fit simulation slice of the simulation of the frequency shift caused by the Meissner effect. On the x-axis is the y-position in μm. On the y-axis is the frequency shift of the cantilever in Hz. The red line shows a best-fit slice is from the simulation at z=12 μm.*

Figure 4.11 shows that the simulation predicts a way higher frequency shift than was measured. Figure 4.12 shows that there is a simulation slice that does fit the measured data, but this slice is from the simulation of 12 μm above the pickup loop instead of 1 μm.

Figure 4.11 shows that the model gives a frequency shift from the cantilever in the order of 10^7 Hz. To get an indication of whether the model works at small distances from the pickup loop, we calculate the cantilever deflection at this height. At a height of 1 μm above the pickup loop, the cantilever will feel a magnetic force of $3.8 \cdot 10^{-8}$ N from the pickup loop. According to Hooke's law, this results in a deflection of the cantilever of 0.5 mm. This is unrealistic for a cantilever with a length of 145 μm.

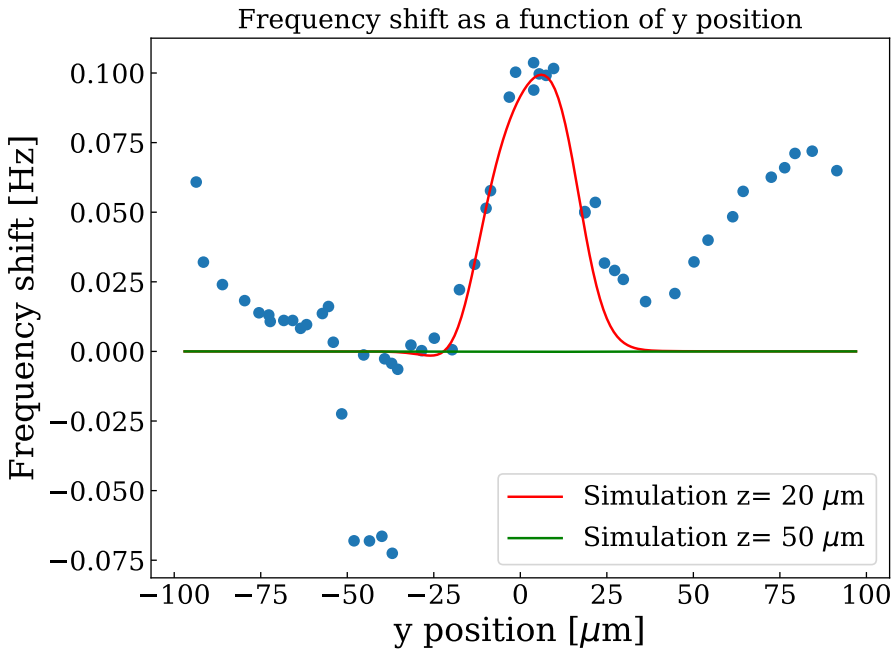

Figure 4.13: *The frequency shift of the cantilever at z=50 μm as a function of y-position compared to different simulation slices from the simulation of the frequency shift caused by the Meissner effect. On the x-axis is the y-position in μm. On the y-axis is the frequency shift of the cantilever in Hz. The green line shows the frequency shift of the cantilever predicted by the simulation at the height of the actual measurements. We see that the simulation shows a lower frequency shift than the frequency shift that was measured. The red line shows the best-fit simulation slice, which is from the simulation at a height of 20 μm.*

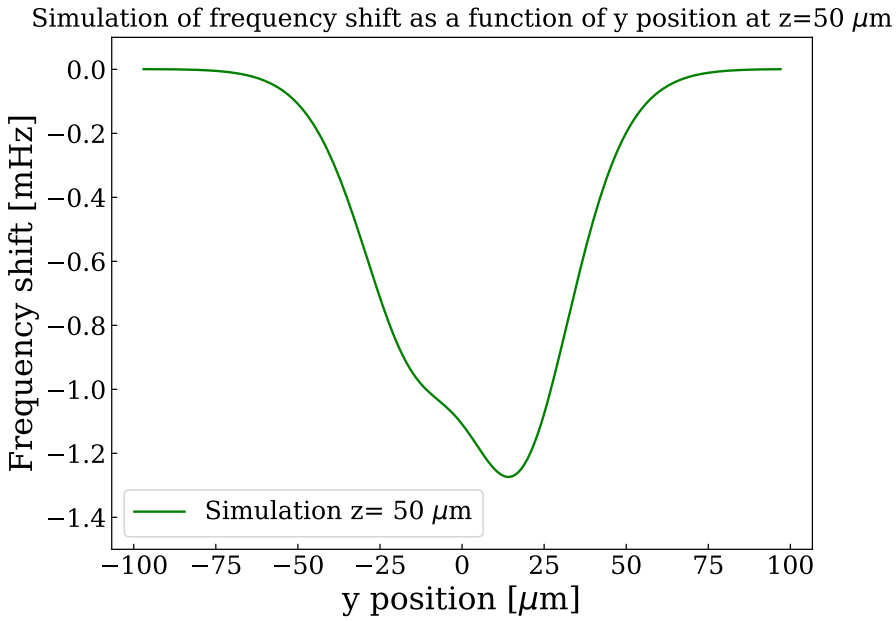

Figure 4.14: *The simulation of the frequency shift of the cantilever at z=50 μm as a function of y-position. On the x-axis is the y-position in μm. On the y-axis is the frequency shift of the cantilever in mHz.*

Figure 4.13 shows that at z=50 μm, the measured frequency shift is larger than the frequency shift predicted by the simulation. It also shows that there is a simulation slice that does fit the data, but that this slice is from the simulation of 20 μm above the pickup loop instead of 50 μm. Figure 4.14 shows that the simulation at z=50 μm shows a negative frequency shift instead of the measured positive one.

Chapter 5

Discussion & Outlook

5.1 Positioning

Based on the results shown in section 4.1, we get values for converting the position of the cantilever from the coordinate system of the capacitor plates to the coordinate system of the simulation. These values are shown in table 5.1. The values in this table are only suitable for this run, as the capacitor plate coordinate system changes each run, but the process described in this thesis can be used for every run.

Coordinate	Conversion
x	+ 158 μm
y	+ 19 μm
z	- 571 μm

Table 5.1: *Results for converting the position of the cantilever from the coordinate system of the capacitor plates to the coordinate system of the simulation.*

However, to better match the measurements from the y-sweep, a scaling factor was applied to the simulation. As part of this rescaling, the simulated values were multiplied by -1, effectively inverting the curve across the x-axis. This suggests that the y-direction in the capacitor plate coordinate system may be inverted. This could also be possible for the x-direction. However, due to the symmetry of the simulation around x=100 μm, there is no indicator for this in the measurements that were done. In future experiments, it could be explored further whether it could indeed be the case that the x- and y-direction are inverted.

It was shown in section 4.1.1 that the coupling of the cantilever is 76.3% of the expected coupling. However, because some assumptions were used during these calculations, the result is deemed reasonable. This is a good indication that the piezo for driving the cantilever works as intended.

5.2 Frequency Uncertainty

5.2.1 Temperature and driving voltage dependence of frequency uncertainty

It was shown in section 4.2.1, in figure 4.6, that the frequency noise decreases when the driving voltage of the cantilever increases. The figure also shows that there seems to be no temperature dependence of the frequency uncertainty. Furthermore, section 4.2.1 shows that the relation between driving voltage of the cantilever and the frequency uncertainty can be described with a $y = a/x$ curve. Thus, the results agree with equation 2.8. The results of this fit are shown in table 4.1. In this table, we can see that the values for a are similar for each fit, which is also in agreement with equation 2.8, as none of the other variables in this equation were changed during the measurements.

5.2.2 Position dependence of frequency uncertainty

It was shown in section 4.2.2, in figure 4.8, that the frequency uncertainty increases in the positive y-direction. No cause of this result was identified. We have also observed an outlier at y= 89 μm, which is y= 108 μm in the coordinate system of the simulation made by Marc de Voogd, and have not been able to identify the cause of this. The only noticeable difference with the rest of the measurements is that this measurement was conducted at the most negative x-position, but only by about half a micrometer. More research about the position dependence of the frequency uncertainty needs to be done. For this, it could be useful to look at positions further from the pickup loop. In this thesis, we only looked at places close to the pickup loop, and if we zoom out more, another relation might become visible. It could also be useful to look at potential noise sources on the sample.

In figure 4.9, we observe that although 4.8 shows a difference in the standard deviation of the uncertainty between the measurements at y=59

μm and y=70 μm, the noise spectra approximately follow the same curve. In contrast, the spectrum of the measurement at y= 81 μm lies significantly above the one from y= 70 μm, despite their standard deviations being relatively similar. We thus see that even though both the uncertainty and the noise increase in the positive y direction, and both have an outlier at y=89 μm, the ratio between the measurements differs for each metric.

5.2.3 Noise bump

A noticeable difference between figure 4.6 and figure 4.8 is that the overall uncertainty in the measurements as a function of position is a lot lower than for the ones as a function of driving voltage. This is because from the start of this run, there was a noise bump around the resonance frequency of our cantilever. The day that we started the measurements of the uncertainty as a function of the y-position, the bump shifted approximately 30 Hz lower, which meant that our results were less influenced by this bump. We did not do anything to our setup that might have caused this change. So even though figure 4.6 now shows no clear relation between temperature and driving voltage, without the noise bump, a relation might become visible. Due to time constraints, it was not possible to repeat these measurements without the noise bump.

5.3 The Meissner effect

Figure 4.11 shows that at a z-position 1 μm above the sample, the simulation that was made using the model described in section 3.7 shows a higher frequency shift than the frequency shift that was measured. It was calculated that this was to be expected, because the force on the cantilever at 1 μm would cause an unrealistic deflection of the cantilever. Figure 4.13 shows that at a height of 50 μm above the sample, the simulation predicts a lower frequency shift than the frequency shift that was measured. Figure 4.14 shows that the simulation shows a negative frequency shift at a height of 50 μm above the sample instead of the positive frequency shift that was measured. Therefore, we can say that the model we chose for the simulation does not give an accurate prediction of the cantilever's frequency shift caused by the Meissner effect. In the future, a new model for simulating the frequency shifts of the cantilever needs to be made.

Version of August 1, 2025– Created August 1, 2025 - 13:51

Chapter 6

Conclusion

In this thesis, we showed a way to determine the position of the cantilever relative to the pickup loop and diamond sample. It was also calculated that the piezo response of the piezo driving the cantilever was 76.3 % of the expected value, this was deemed sufficient proof that the piezo works as intended.

We showed a $y = a/x$ relation between the driving voltage of the cantilever and the frequency uncertainty of the cantilever. We also showed a relation between the y-position of the cantilever above the sample and the frequency uncertainty of the cantilever. No relation between the temperature of the experiment and the frequency uncertainty of the cantilever was found.

Finally, we showed that the model used to simulate the cantilever's frequency shift due to the Meissner effect of the superconducting pickup loop did not match the measured frequency shifts.

Acknowledgements

I would like to thank Tjerk Oosterkamp for allowing me to be part of his research group. I had an amazing time and learned a lot. I would especially like to thank Loek, thank you for being my daily supervisor and trusting me with your experiment. You taught me a lot and always made me feel included. I would also like to thank the other PhD students in the Oosterkamp group, Jurriaan, Dennis, and Koen, for their input on various aspects of my project.

Lastly, I would like to thank all the bachelor and master students of the Oosterkamp group: Lianne, Winesh, Thijmen, Mart, Nathaniel, Bram, Marnix, and Patrick, as well as the entire Hensen group, for all the fun conversations in the lab and during lunch breaks.

Bibliography

[1] A. Bassi, K. Lochan, S. Satin, T. P. Singh, and H. Ulbricht, *Models of wave-function collapse, underlying theories, and experimental tests*, Reviews of Modern Physics **85**, 471â527 (2013).

[2] A. Einstein et al., *The foundation of the general theory of relativity*, Annalen Phys **49**, 769 (1916).

[3] J. B. Hartle, *Gravity: An Introduction to Einsteinâs General Relativity*, Cambridge University Press, 2021.

[4] M. Fuwa, S. Takeda, M. Zwierz, H. M. Wiseman, and A. Furusawa, *Experimental proof of nonlocal wavefunction collapse for a single particle using homodyne measurements*, Nature Communications **6**, 6665 (2015).

[5] D. Savickas, *Relations between Newtonian Mechanics, general relativity, and quantum mechanics*, American Journal of Physics **70**, 798 (2002).

[6] L. Diósi, *Gravitation and quantum-mechanical localization of macro-objects*, Physics Letters A **105**, 199â202 (1984).

[7] J. Plugge, *Probing the Limits of Quantum Mechanics using a Cold Mechanical Force Sensor*, PhD thesis, Leiden University, 2025.

[8] D. Rugar, R. Budakian, H. Mamin, and B. Chui, *Single spin detection by magnetic resonance force microscopy*, Nature **430**, 329 (2004).

[9] H. Mamin and D. Rugar, *Sub-attonewton force detection at millikelvin temperatures*, Applied Physics Letters **79**, 3358 (2001).

[10] O. Usenko, A. Vinante, G. Wijts, and T. Oosterkamp, *A superconducting quantum interference device based read-out of a subattonewton force*

sensor operating at millikelvin temperatures, Applied Physics Letters **98** (2011).

[11] M. Ruf, M. IJspeert, S. Van Dam, N. De Jong, H. Van Den Berg, G. Evers, and R. Hanson, *Optically coherent nitrogen-vacancy centers in micrometer-thin etched diamond membranes*, Nano letters **19**, 3987 (2019).

[12] D. J. Griffiths, *Introduction to Electrodynamics*, Cambridge University Press, 4 edition, 2017.

[13] G. Ludwig, *Electron Spin Resonance: Its use is leading to a new understanding of impurity centers in semiconductors such as silicon.*, Science **135**, 899 (1962).

[14] M. de Wit, *Advances in SQUID-detected magnetic resonance force microscopy*, PhD thesis, Leiden University, 2019.

[15] M. de Voogd, *MRFM and the Spin Bath*, PhD thesis, Leiden University, 2018.

[16] A. Haque and S. Sumaiya, *An overview on the formation and processing of nitrogen-vacancy photonic centers in diamond by ion implantation*, Journal of Manufacturing and Materials Processing **1**, 6 (2017).

[17] W. Meissner and R. Ochsenfeld, *Ein neuer effekt bei eintritt der supraleitfähigkeit*, Naturwissenschaften **21**, 787 (1933).

[18] R. Feynman, *The Feynman Lectures on Physics Vol. III Ch. 21: The Schrödinger Equation in a Classical Context: A Seminar on Superconductivity*.

[19] J. Bardeen, L. N. Cooper, and J. R. Schrieffer, *Theory of superconductivity*, Physical review **108**, 1175 (1957).

[20] J. Wagenaar et al., *Probing the nuclear spin-lattice relaxation time at the nanoscale*, Physical Review Applied **6**, 014007 (2016).

[21] F. J. Giessibl, F. Pielmeier, T. Eguchi, T. An, and Y. Hasegawa, *Comparison of force sensors for atomic force microscopy based on quartz tuning forks and length-extensional resonators*, Physical Review BâCondensed Matter and Materials Physics **84**, 125409 (2011).

[22] Z. Instruments, *Principles of lock-in detection and the state of the art*, CH-8005 Zurich, Switzerland, Accessed (2016).

[23] Z. Instruments, *Phase-Locked Loops for Analog Signals*, CH-8005 Zurich, Switzerland, Accessed (2022).

[24] A. M. J. den Haan, G. H. C. J. Wijts, F. Galli, O. Usenko, G. J. C. van Baarle, D. J. van der Zalm, and T. H. Oosterkamp, *Atomic resolution scanning tunneling microscopy in a cryogen free dilution refrigerator at 15 mK*, Review of Scientific Instruments **85** (2014).

[25] R. Regter, *Spin Density Determination by means of LowTemperature Magnetic*, Bachelor's thesis, Leiden University, 2023.

[26] B. W. Chui, Y. Hishinuma, R. Budakian, H. J. Mamin, T. W. Kenny, and D. Rugar, *Mass-loaded cantilevers with suppressed higher-order modes for magnetic resonance force microscopy*, in *TRANSDUCERS'03. 12th International Conference on Solid-State Sensors, Actuators and Microsystems. Digest of Technical Papers (Cat. No. 03TH8664)*, volume 2, pages 1120–1123, IEEE, 2003.

[27] E. Nazaretski, J. D. Thompson, R. Movshovich, M. Zalalutdinov, J. Baldwin, B. Houston, T. Mewes, D. Pelekhov, P. Wigen, and P. Hammel, *Temperature-dependent magnetic resonance force microscopy studies of a thin Permalloy film*, Journal of applied physics **101** (2007).

[28] W. Bosch, *Hightech Development Leiden*.